Supplementary Information (SI) for Materials Advances.

Electronic supporting Information

Stabilization of nesquehonite for application in carbon capture utilization and storage

Nirrupama Kamala Ilango[a], Hoang Nguyen[a], Mohammad Alzeer[a], Frank Winnefeld[b], Paivo Kinnunen*[a]

[a] Fibre and Particle Engineering Research Unit, University of Oulu, Pentti Kaiteran katu 1, 90014 Oulu, Finland

[b] Swiss Federal Laboratories for Materials Science and Technology (Empa), Laboratory for Concrete & Asphalt, Überlandstrasse 129, 8600 Dübendorf, Switzerland

*Corresponding author (Email address: paivo.kinnunen@oulu.fi)

Methods

Materials

Magnesium hydroxide [$Mg(OH)_2$] of assay 95-100.5% from VWR chemicals with a D_{50} of about 8 μm was used to synthesize nesquehonite. The schematical representation of nesquehonite synthesis is shown in Fig. S3 The commercial pH 7 buffer based on phosphate from VWR chemicals was used in this study. The materials used to prepare pH buffer solutions: Potassium dihydrogen phosphate (KH_2PO_4, assay 99.5 - 100.5%) and hydrochloric acid (HCl) solution of 0.1 mol/l were from VWR chemicals, sodium hydroxide (NaOH, ≥ 98 %, pellets) and tris (hydroxy methyl) aminomethane [$(HOCH_2)_3CNH_2$, ≥ 99.8 %] were from Sigma-Aldrich.

Preparation of pH 7 buffers

Two pH 7 buffers based on the following method were prepared for the study.

1. **pH 7 - phosphate** based: 100 ml of 0.1 M KH_2PO_4 was added to 58.2 ml of 0.1 M NaOH, and the solution was made to 200 ml with distilled water.
2. **pH 7 - amine** based: 100 ml of 0.1 M tris (hydroxy methyl) aminomethane ($(HOCH_2)_3CNH_2$) was added to 93.2 ml of 0.1 M HCl, and the solution was made up to 200 ml with distilled water.
3. Buffer solutions were equilibrated at room temperature in sealed conditions for 2 days prior to their use.

The pH of the solution was measured using a Hach HQd portable pH meter and IntelliCAL pHC281 probe. The measurements were done at room temperature of about 23 ± 2 °C, calibration was done using standard pH solutions before the measurements.

Characterization methods

X-ray powder diffraction (XRD) was performed using a Rigaku SmartLab equipped with a CoKα source operated at 40 kV and 135 mA. The measurements were conducted at a scan rate of 3 °/min in the range 5 ° to 90 ° 2θ with a step size of 0.02 °/ step.

Thermogravimetric analysis (TGA) was performed with SDT 650 (TA instruments) to measure the decomposition of samples. The temperature was increased from 30 °C to 980 °C with a ramp of 10 K/min in an N_2 atmosphere. The decarbonation of nesquehonite occurs at the temperature range of 350 – 600 °C and was used to quantify the phase using the following equation [1]:

$$m_{MgCO_3 \cdot 3H_2O} = m_{350-600\,^{\circ}C} \times \frac{M_{MgCO_3 \cdot 3H_2O}}{M_{CO2}}$$

where, $m_{350\text{-}600\,^{\circ}C}$ = mass loss in the temperature range between 350-600 °C obtained from TGA and M = molecular weights of nesquehonite and CO_2.

The morphologies of the pastes were studied using field emission scanning electron microscopy (FESEM; ZEISS Sigma device). The images were taken with an accelerating voltage of 5 kV and in secondary electron mode with EDAX detector. Platinum sputtering was done to reduce charging. Energy dispersive X-ray analysis (EDS) was done on selected samples using Zeiss Ultra Plus (Germany) with a 15 kV accelerator voltage and a working distance of 8.5 – 9 mm. The filtered precipitates were pressed into a solid disc using a hydraulic press (5 tons), the cross-section of the disc was then impregnated with epoxy resin and polished using finally a 1 μm diamond paste. The polished section was then coated with carbon, and the elemental composition was mapped using an X-Max EDS detector in backscattered electron (BSE) mode. Further hypermaps and their corresponding Quant Maps were acquired using Oxford Instrument Aztec software (the UK) with a resolution of 1024 × 768 pixels and a dwell

time of 200 µs for a total of 10 frames. The edxia [2] method in the Glue [3] interface was used to analyze the acquired hypermaps.

GEMS, a thermodynamic modeling software based on the Gibbs free energy minimization method [4,5] along with the database for relevant phases [6,7] was used for the thermodynamic calculation in this study. The Cemdata 18 [8], developed specifically for cementitious binders, the phosphate database [7,9–12] which consists of hydrated phases found commonly in hydrated magnesium and calcium phosphate cement, the database for several hydrated magnesium carbonates compiled from various sources [13–16] and as tabulated by [6] along with the PSI/Nagra database in GEMS was used. GEMS was used to study the thermodynamically stable phases in the system (Fig. S7). Magnesite formation at ambient conditions is kinetically hindered and requires elevated temperature and pressure [17,18] and hence its precipitation was restricted. The thermodynamic stability of magnesium complexes with phosphate and carbonates in an aqueous medium with the pH varying from 6 to 12 by allowing only the precipitation of nesquehonite to mimic the original system (Fig. S8) was also done with the help of GEMS. The mix recipe used for the model was based on a scaled up experimental system; water – 100 g, KH_2PO_4 – 0.7 g, NaOH – 0.12 g and nesquehonite – 10 g.

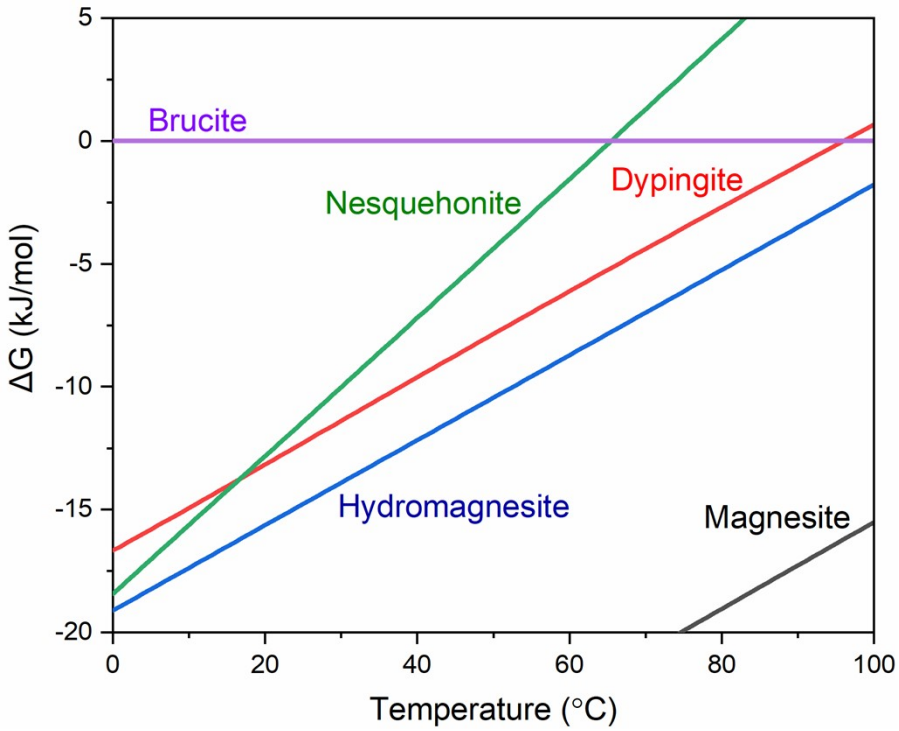

Figure S1. The figure represents the relative thermodynamic stabilities of various HMCs with respect to brucite as a function of temperature at saturated conditions and a partial CO_2 pressure of 1%, as adapted from [19]. The line at 0 kJ/mol represents the free energy of brucite.

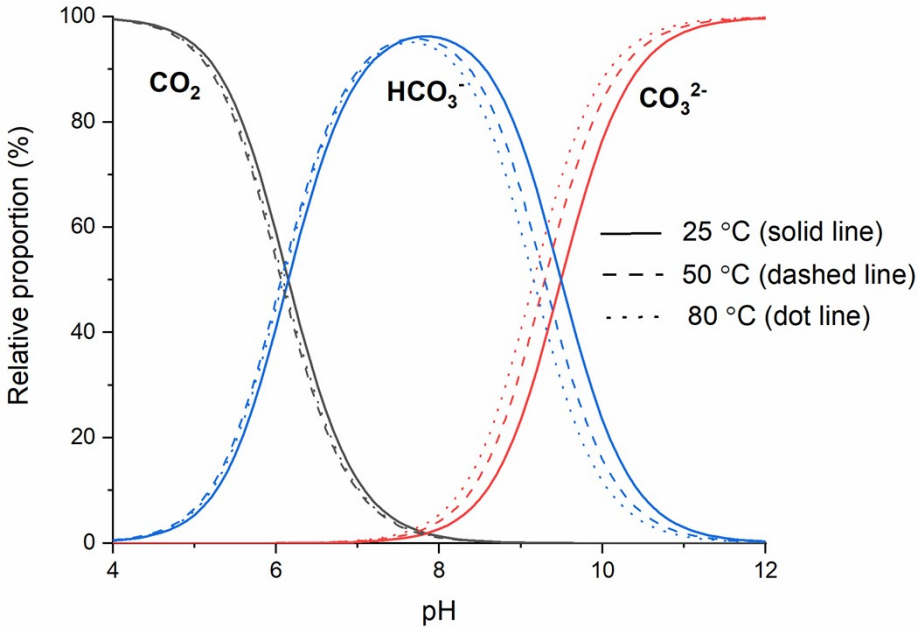

Figure S2. The relative amount of CO_2 speciation in water at varying pH from 4 to 12. The maximum concentration of bicarbonate ions is centered around pH 8. The shift in CO_2 speciation with temperature (at 25, 50 and 80 °C) is also depicted. The data is obtained from calculations made with GEMS, thermodynamic software by adding 1 g CO_2 in 10 g water in a closed system and by varying the pH by titration method.

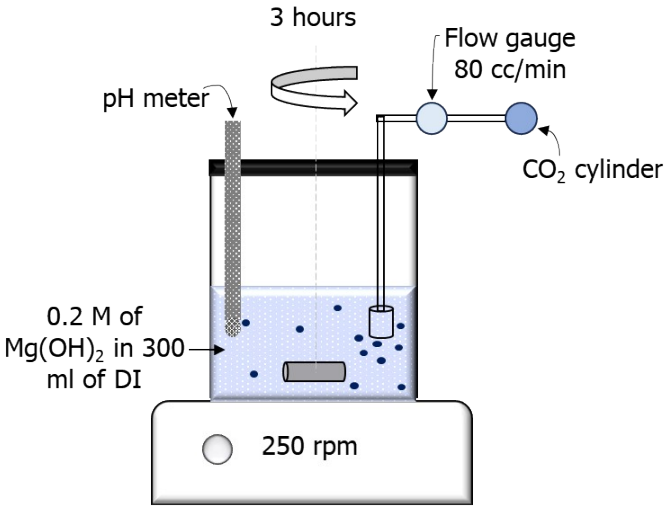

Figure S3. Laboratory set-up for nesquehonite synthesis. 0.2 M of $Mg(OH)_2$ (11.6 g) from VWR chemicals was added to 300 ml of deionized water. CO_2 gas (purity ≥ 99.8 %) released at a pressure of 1 bar (T = 23 ± 2 °C) was bubbled into the slurry at a flow rate of 80 cc/min for 3 hours. The pH of the slurry was measured every 15 mins and it stabilized to about 7.2 at the end of the reaction. The slurry was then filtered, washed with isopropanol followed by diethyl ether, and dried at 40 °C for 20 mins.

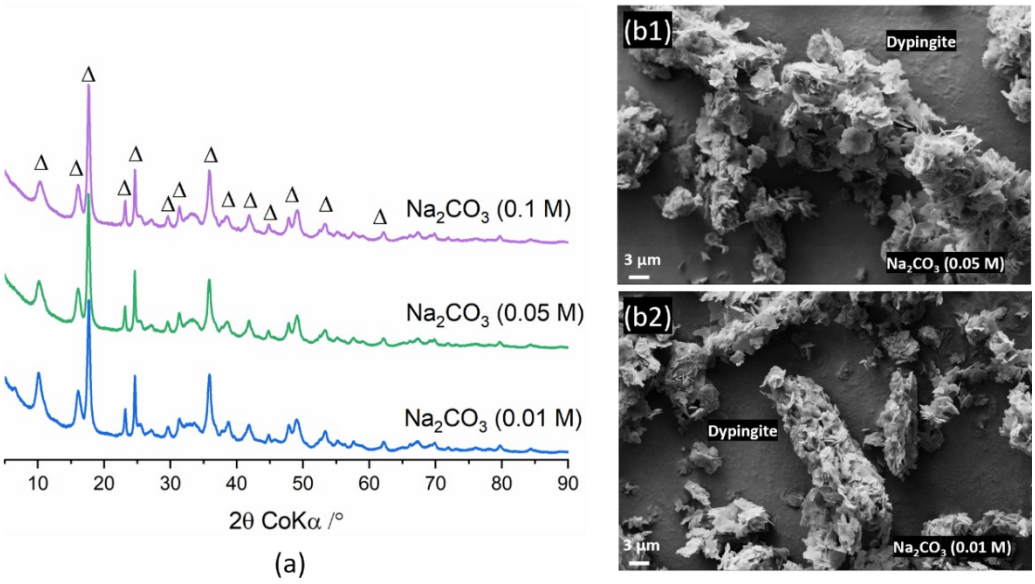

Figure S4. (a)X-ray diffraction pattern of nesquehonite aged in different concentrations of sodium carbonate solutions along with the (b1 and b2) morphology as seen from SEM. Δ indicates dypingite. It could be observed that complete conversion of nesquehonite to dypingite is observed in all concentrations of sodium carbonate solution aged at 50 °C for 10 days.

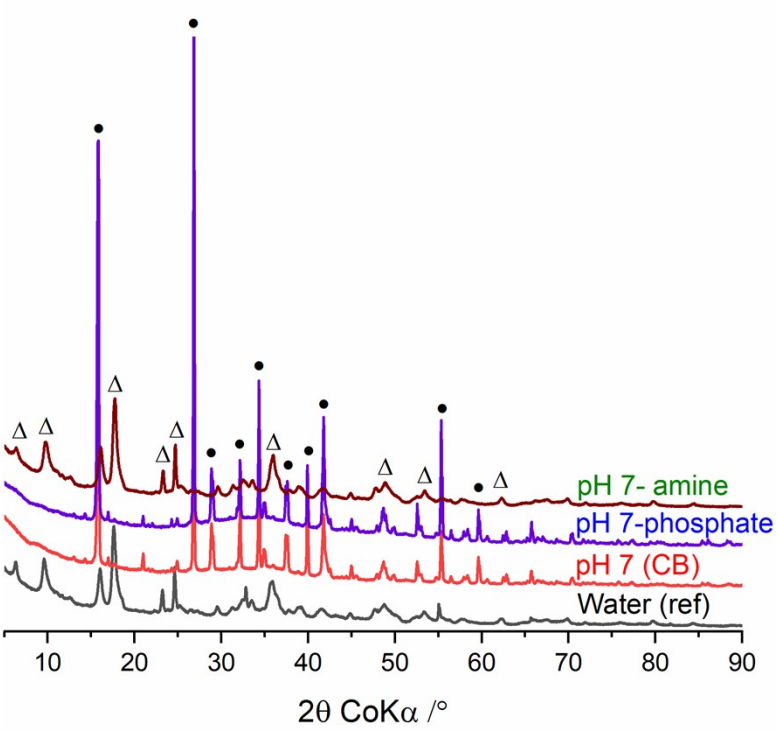

Figure S5. Diffraction pattern of nesquehonite aged for 7 days in water and the buffer solutions at 50 °C. In phosphate based commercial (pH 7 (CB)) and lab made buffer (pH 7 – phosphate) solutions, the characteristic reflections of nesquehonite at 15.80 (6.50 Å), 21. 01 (4.90 Å), 26.86 (3.85 Å), 32.16 ° 2θ (3.22 Å) are observed, indicating its presence. In addition to nesquehonite, a hump between 25 - 42 °2θ is also observed which could

indicate the presence of an amorphous phase. In the case of water and pH 7 – amine buffer solution, we observe a complete conversion of the phase to dypingite.

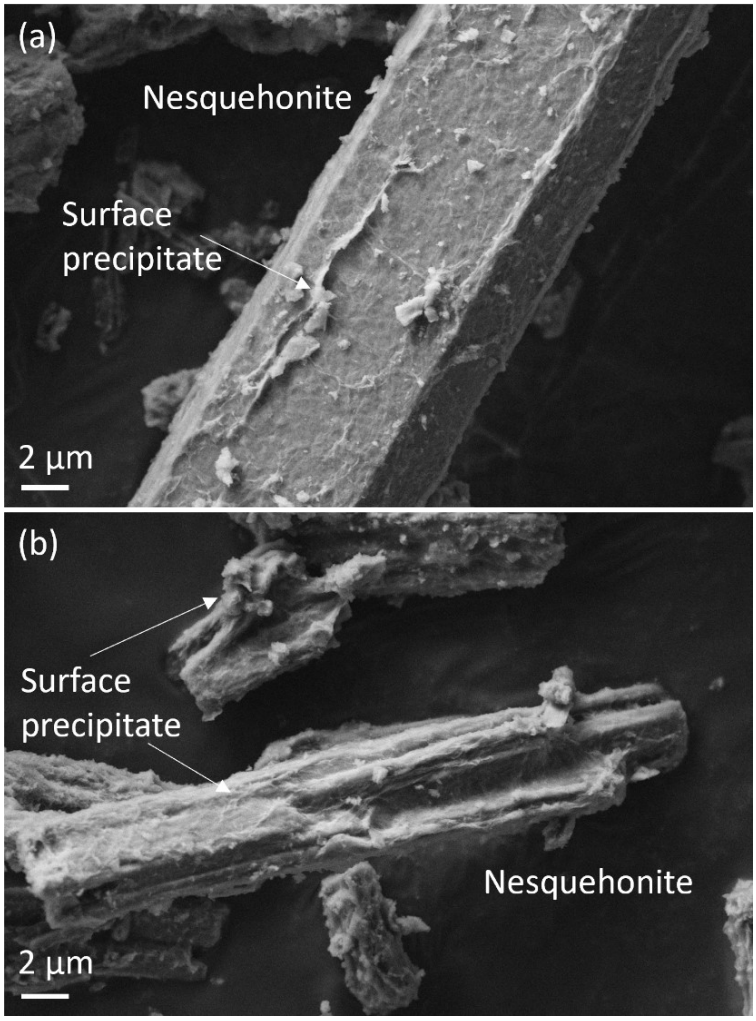

Figure S6. (a) and (b) SEM images of nesquehonite aged in the lab made pH 7 phosphate buffer (pH 7- phosphate) for 28 days at 50 °C, showing the precipitation of a phase on the surface of nesquehonite, that could possibly hinder further reaction, thereby stabilizing nesquehonite.

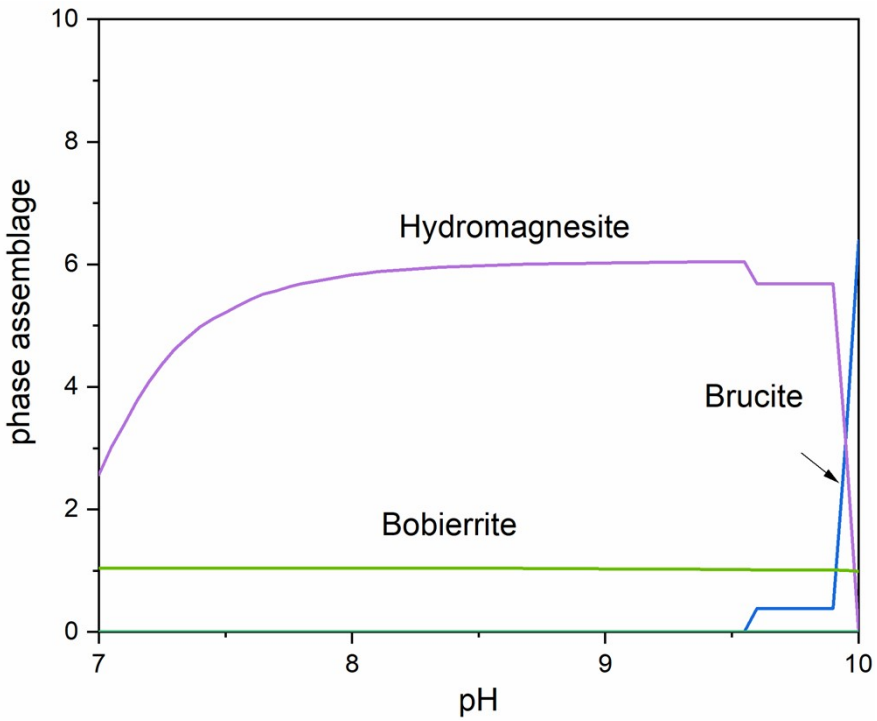

Figure S7. Phase assemblage of the system at equilibrium as predicted by GEMS. It can be observed that bobierrite ($Mg_3(PO_4)_2 \cdot 8H_2O$) is the most stable magnesium phosphate phase in the system for the calculated pH range. Hydromagnesite is the stable phase HMC to precipitate, however, experimentally we still observe nesquehonite after 28 days. These observations indicate that the magnesium phosphate phase forms on the nesquehonite surface and prevents its conversion to hydromagnesite and/or dypingite. The formation of low soluble calcium phosphate phases on cement surfaces was reported earlier [20].

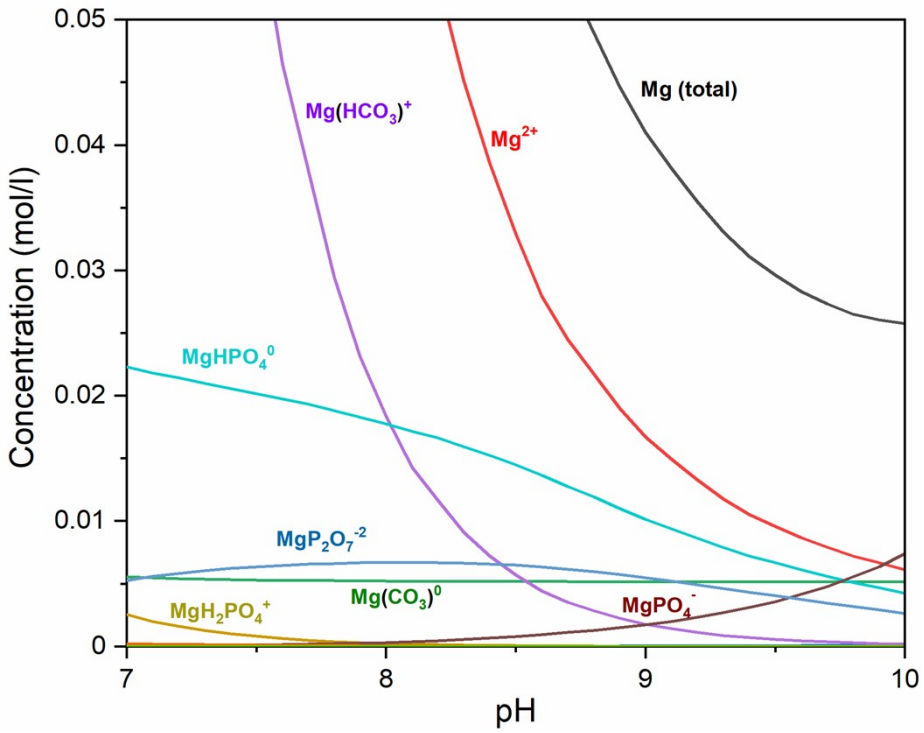

Figure S8. Complexation of Mg with phosphate and carbonates in an aqueous media. The calculations were made for the system allowing the precipitation of only nesquehonite to mimic the experimental observations. It can be observed that the aqueous speciation of magnesium complexes with phosphate and carbonates varies with the pH of the solution. With $MgHPO_4^0$ being the most preferred speciation in the relevant pH of about 9.2, along with $MgP_2O_7^{-2}$ and $Mg(CO_3)^0$ and $MgPO_4^-$ at a pH greater than 10.

SI References

1 B. Lothenbach, P. Durdziński and K. D. Weerdt, in *A Practical Guide to Microstructural Analysis of Cementitious Materials*, 2016, pp. 177–211.
2 F. Georget, W. Wilson and K. L. Scrivener, *Cement and Concrete Research*, 2021, **141**, 106327.
3 T. Robitaille, C. Beaumont, P. Qian, M. Borkin and A. Goodman, *Zenodo*, , DOI:10.5281/zenodo.3385920.
4 D. A. Kulik, T. Wagner, S. V. Dmytrieva, G. Kosakowski, F. F. Hingerl, K. V. Chudnenko and U. R. Berner, *Comput Geosci*, , DOI:10.1007/s10596-012-9310-6.
5 T. Wagner, D. A. Kulik, F. F. Hingerl and S. V. Dmytrieva, *The Canadian Mineralogist*, 2012, **50**, 1173–1195.
6 E. Bernard, B. Lothenbach, D. Rentsch, A. German and F. Winnefeld, *Mater Struct*, 2022, **55**, 183.
7 B. Lothenbach, B. Xu and F. Winnefeld, *Applied Geochemistry*, 2019, **111**, 104450.
8 B. Lothenbach, D. A. Kulik, T. Matschei, M. Balonis, L. Baquerizo, B. Dilnesa, G. D. Miron and R. J. Myers, *Cement and Concrete Research*, 2019, **115**, 472–506.
9 Empa - Concrete & Asphalt - Phosphate data, https://www.empa.ch/web/s308/phosphate-data, (accessed February 8, 2024).
10 B. Xu, B. Lothenbach and F. Winnefeld, *Cement and Concrete Research*, 2020, **131**, 106012.
11 B. Xu, F. Winnefeld and B. Lothenbach, *Cement and Concrete Research*, 2021, **142**, 106370.
12 B. Xu, F. Winnefeld, B. Ma, D. Rentsch and B. Lothenbach, *Cement and Concrete Research*, 2022, **156**, 106788.
13 Q. Gautier, P. Bénézeth, V. Mavromatis and J. Schott, *Geochimica et Cosmochimica Acta*, 2014, **138**, 1–20.
14 A. L. Harrison, V. Mavromatis, E. H. Oelkers and P. Bénézeth, *Chemical Geology*, 2019, **504**, 123–135.
15 H. Helgeson, J. Delany, H. Nesbitt and D. Bird, 1978.
16 A. M. Chaka and A. R. Felmy, *J. Phys. Chem. A*, 2014, **118**, 7469–7488.
17 F. L. Sayles and W. S. Fyfe, *Geochimica et Cosmochimica Acta*, 1973, **37**, 87–99.
18 V. Prigiobbe and M. Mazzotti, *Chemical Engineering Journal*, 2013, **223**, 755–763.
19 B. Lothenbach, E. Bernard, A. German and F. Winnefeld, *ce/papers*, 2023, **6**, 342–356.
20 H. Pasco, S. Naidu, B. Lothenbach and E. Sassoni, *Cement and Concrete Composites*, 2023, **141**, 105124.